ISSN 2072-5981
doi: 10.26907/mrsej

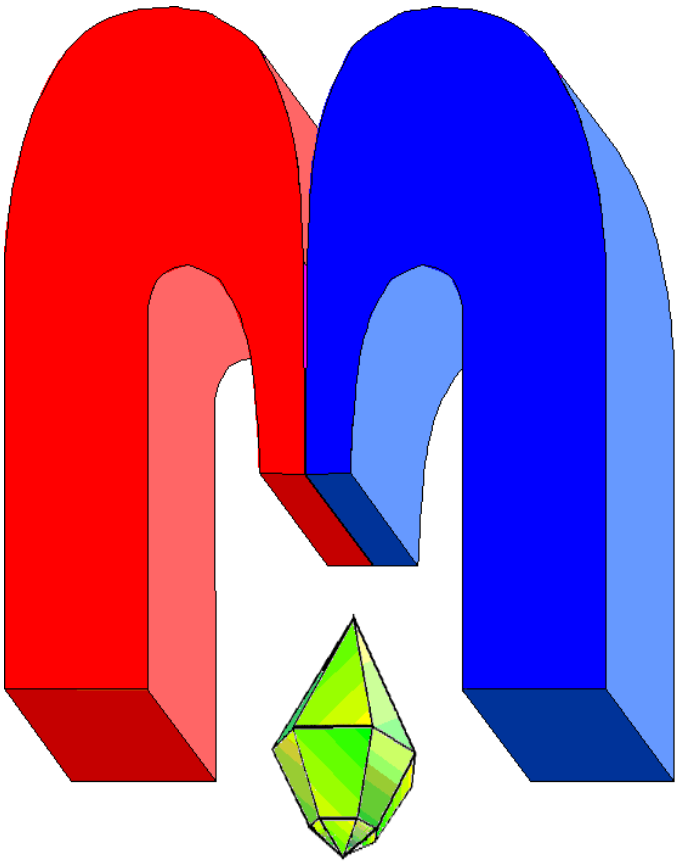

Magnetic Resonance in Solids

Electronic Journal

Volume ***21***
Issue ***5***
Paper No ***19502***
1-11 pages
2019
doi: **10.26907/mrsej-19502**

http://mrsej.kpfu.ru
http://mrsej.ksu.ru

Established and published by Kazan University
Endorsed by International Society of Magnetic Resonance (ISMAR)
Registered by Russian Federation Committee on Press (#015140),
August 2, 1996
First Issue appeared on July 25, 1997

"***Magnetic Resonance in Solids. Electronic Journal***" (**MRS*ej***) is a peer-reviewed, all electronic journal, publishing articles which meet the highest standards of scientific quality in the field of basic research of a magnetic resonance in solids and related phenomena.

Indexed and abstracted by
Web of Science (*ESCI*, Clarivate Analytics, from 2015), *Scopus* (Elsevier, from 2012), *RusIndexSC* (*eLibrary*, from 2006), *Google Scholar*, *DOAJ*, *ROAD*, *CyberLeninka* (from 2006), *SCImago Journal & Country Rank*, etc.

Technical Editor
Maxim **Avdeev** (KFU)

* In Kazan University the Electron Paramagnetic Resonance (EPR) was discovered by Zavoisky E.K. in 1944.

A variable temperature EPR study of Cu^{2+} doped single crystals of pyrovanadates β-$Mg_2V_2O_7$, α-$Zn_2V_2O_7$: estimations of non-coincident $\tilde{\mathbf{g}}^2$- and $\tilde{\mathbf{A}}^2$-tensors

S.K. Misra[1,*], S.I. Andronenko[2,**]

[1]Physics Department, Concordia University, Montreal, QC, H3G 1M8, Canada

[2]Institute of Physics, Kazan Federal University, Kremlevskaya 18, Kazan 420008, Russia

[*]*E-mail: sushil.misra@concordia.ca*

[**]*E-mail: SIAndronenko@kpfu.ru*

(Received July 2, 2019; revised July 20, 2019;
accepted July 22, 2019; published July 31, 2019)

Full angular variations of Cu^{2+} EPR spectra in β-$Mg_2V_2O_7$ (MgVO) and α-$Zn_2V_2O_7$ (ZnVO) were recorded for orientations of external magnetic field in three mutually perpendicular planes at 120 K and 295 K, as well as in temperature range from 110 to 295 K at some chosen orientations of magnetic field. The principal values of the $\tilde{\mathbf{g}}^2$- and $\tilde{\mathbf{A}}^2$-tensors, as well as the orientations of their principal axes were determined from angular variations of EPR line positions in three mutually perpendicular planes, using a rigorous least square fitting procedure, especially adapted to the case of non-coincident principal axes of the $\tilde{\mathbf{A}}^2$-tensors for the monoclinic and triclinic point-group symmetries in MgVO and ZnVO crystals, respectively. This procedure uses the eigenvalues and eigenvectors of the spin-Hamiltonian matrix, which allows to determine the orientations of the principal axes of the $\tilde{\mathbf{g}}^2$ (Zeeman) and $\tilde{\mathbf{A}}^2$ (hyperfine-interaction)-tensors. It is found, that the principal values of $\tilde{\mathbf{g}}^2$- and $\tilde{\mathbf{A}}^2$-tensors of the Cu^{2+} ions are similar in the two crystals; however, the orientations of the principal axes of these tensors are significantly different from each other. This is because the Cu^{2+} ion in MgVO is 6-fold coordinated, whereas it is 5-fold coordinated in trigonal bipyramidal coordination in ZnVO. The principal values of the $\tilde{\mathbf{g}}^2$-tensor, so obtained, are exploited to determine the electronic ground state of the Cu^{2+} ion in these two crystals.

PACS: 75.10.Dg, 76.30.-v, 75.20
Keywords: pyrovanadates, EPR, Cu^{2+}, spin-Hamiltonian parameters

1. Introduction

Mixed vanadium oxides, such as V-Mg-O, V-Zn-O are important in catalytic processes such as oxidative dehydrogenation and hydrocarbons [1] and selective catalytic reduction of NO by ammonia [2, 3]. The vanadates are of great interest at present, because they have a variety of applications, e.g., use in the synthesis of the supported V_2O_7 catalyst [4], insulin-mimetic agents [5] and rechargeable Li batteries [6–8]. The vanadates are prospective materials for supercapacitors [9], photocatalysts [10], and gas sensors [11]. Furthermore, the thermochromic nature of α-$Zn_2V_2O_7$ (ZnVO hereafter) is of interest. This crystal is light yellow in the α phase and changes to red in the β phase [12]. Ioffe *et al.* [13] found that the electric conductivity of β-$Mg_2V_2O_7$ (MgVO hereafter) and ZnVO pyrovanadates depends strongly on the impurity ions and thermal treatment, which dictates the formation of defects. Crystallography of these compounds was studied experimentally by solid-state NMR [14–16], and theoretically, by using the point-monopole approximation and *ab-initio* calculations [16, 17]. For relevance, it is noted, that the Mn^{2+} EPR in single crystals of $Cd_2V_2O_7$ was investigated by Stager [18], whereas those in single crystals of $Ca_2V_2O_7$ and $Mg_2V_2O_7$ by Ioffe *et al.* [19]. Later, the Mn^{2+} EPR spectra in α-$Zn_2V_2O_7$ single crystals were investigated by multifrequency EPR by Misra *et al.* [20]. The V^{4+} EPR study in single crystals of MgVO and ZnVO were reported recently by Misra *et al.* [21].

The use of nanoparticles of vanadium oxides as supported monolayer vanadia catalysts [22] has attracted great interest recently because of its enhanced effectiveness in nano-state as compared to that in bulk-state materials. The doping of, e.g. MgVO, by transition-metal ions (Mn, Co, Ni, Fe) also increases its catalytic effectiveness [23]. As a consequence, study of different impurity ions in these compounds is very important to understand the effectiveness of catalytic properties of these oxides. In this paper, Cu^{2+} EPR spectra in MgVO and ZnVO are presented at various selected temperature in the range 110 - 295 K, along with full angular variations of EPR line positions in three mutually perpendicular planes at 120 and 295 K. From these latter, the principal values and the orientations of their principal axes of the $\tilde{\mathbf{g}}^2$- and $\tilde{\mathbf{A}}^2$-tensors of the Cu^{2+} ion in MgVO and ZnVO single crystals are estimated using a rigorous least-squares fitting (LSF) procedure, employing the eigenvalues and eigenvectors as obtained by the diagonalization of the spin-Hamiltonian matrix. The principal g values, so obtained, are exploited to determine the electronic ground state of the Cu^{2+} ion in these two crystals.

2. Crystal structure

The growth habits of MgVO and ZnVO single crystals are shown in Fig. 1. The crystals are found to be twinned, as determined by X-ray diffraction. The synthesis of β-$Mg_2V_2O_7$ and α-$Zn_2V_2O_7$ single crystals was described in [21]. The Cu impurity was added in the form of 0.1 mol % CuO to initial chemical reagents. The ionic radii of several ions in 6-fold and 5-fold co-ordinations were listed and analyzed by Shannon [24]. In the Pauling model, where the ionic radius of O^{2-} was taken as 1.40 Å, the ionic radii of the Mg^{2+} and Cu^{2+} ions are 0.72 Å and 0.73 Å in the octahedral coordination, respectively. The ionic radii of Zn^{2+} and Cu^{2+} are 0.68 Å and 0.65 Å in the 5-fold coordination, respectively. Therefore, the Cu^{2+} ion substitutes for the Mg^{2+} and Zn^{2+} ions in the corresponding coordination practically without any distortions of the polyhedron.

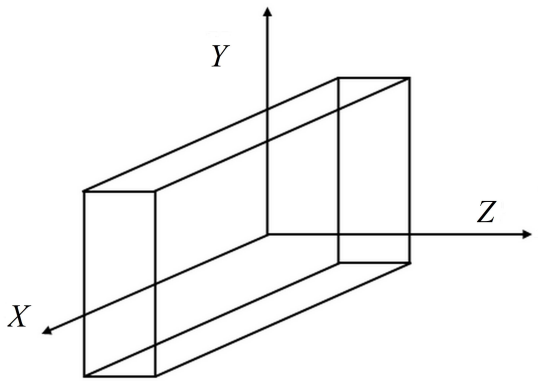

Figure 1. The growth habits of β-$Mg_2V_2O_7$ and α-$Zn_2V_2O_7$ single crystals

ZnVO. As the temperature lowered, $Zn_2V_2O_7$ undergoes a fast reversible structural phase transformation at 615° C from the high-temperature thortveitite β phase (HT phase)with the space group $C2/m$ to the low-temperature α phase (LT phase)of $Zn_2V_2O_7$, characterized by the space group $C2/c$ with the unit-cell parameters: $a = 7.429$ Å, $b = 8.340$ Å, $c = 10.098$ Å and $\beta = 114.4°$; $Z = 4$ [25]. The structure of α-$Zn_2V_2O_7$ was shown in Fig. 2. The difference between the high (HT) and low (LT) temperature phase structures of $Zn_2V_2O_7$ crystal is that in the former the coordination of Zn ions is six-fold, whereas in the latter the cations reduce their coordination to five oxygen atoms, as seen from Fig. 2. In the LT-phase, the ZnO_5 group is a distorted trigonal bipyramid, with the longer Zn-O bonds oriented in the axial direction. In the

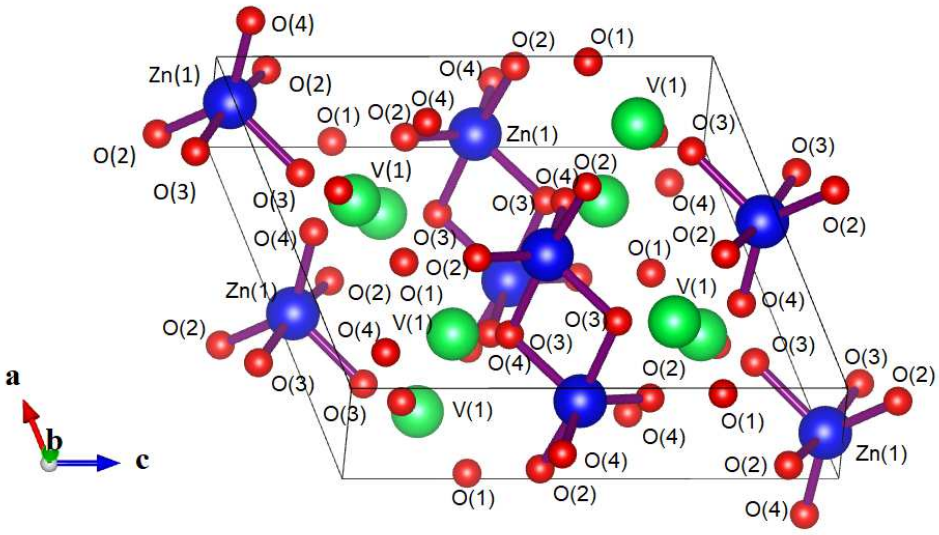

Figure 2. The structure of the α-$Zn_2V_2O_7$.

LT-structure of α-$Zn_2V_2O_7$ crystal, the vanadium and oxygen ions form V_2O_7 pyrogroups; layers of oxygen atoms are stacked perpendicular to the [001] axis, and Zn ions and V-O-V groups lie in octahedrally coordinated sites in alternate layers of oxygen ions. The point symmetry of the Zn^{2+} ion is C_i and there is only one physically inequivalent site for Zn^{2+} ions, which is 5-fold coordinated to oxygen ions. The bond lengths to these oxygen ions are from 1.973 Å to 2.087 Å. The sixth bonded oxygen ion lies 3.35 Å away from the Zn ion.

MgVO. The high-temperature β-phase of $Mg_2V_2O_7$ was synthesized at higher temperatures, $T > 800°$ C, which is above the phase transition between α- and β-phases, at $T = 760°$ C [26]. This phase is stable at room temperature and possesses triclinic space symmetry $P\bar{1}$, with the

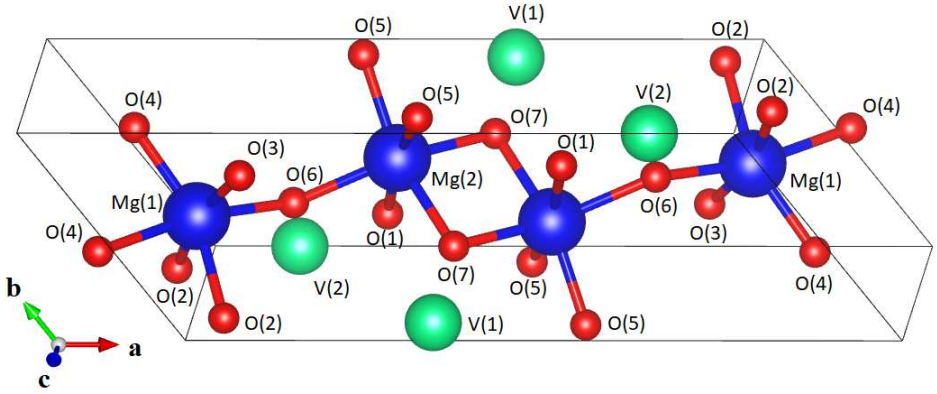

Figure 3. The structure of the β-$Mg_2V_2O_7$.

unit-cell parameters: $a = 13.767$ Å, $b = 5.414$ Å, $c = 14.912$ Å and $\alpha = 81.42°$, $\beta = 106.82°$, $\gamma = 130.33°$; $Z = 2$ [27]. The structure of of β-$Mg_2V_2O_7$ in the HT-phase, shown in Fig. 3, consists of chains of V_2O_7 groups formed from two VO_4 tetrahedra, which share one common oxygen ion. The adjacent V_2O_7 chains form sheets lying in the (001) plane. They are separated by Mg cations which share oxygen atoms with these sheets. The point symmetry of the Mg ion in HT-phase β-$Mg_2V_2O_7$ is C_i and there exist two physically inequivalent sites for Mg^{2+} ions, both are 6-fold coordinated with similar Mg-O bonding lengths, which range from 1.992 Å to 2.083 Å with only one at 2.246 Å. All of these are terminal oxygen atoms in the case of Mg(1),

as shown in Fig. 3 whereas one of the oxygen atoms bonded to Mg(2)ion is a bridging oxygen atom. The bond lengths for the Mg(2) ion varies from 2.049 Å to 2.221 Å. Each MgO_6 groups shares two edges.

3. Cu^{2+} EPR spectra and estimation of values of the matrix elements of $\tilde{g}^2$- and $\tilde{A}^2$-tensors

Experimental arrangements. A Bruker ER-200D SRC EPR X-band (9.6 GHz) spectrometer equipped with a nitrogen-flow Bruker variable temperature accessory was used to record the EPR spectra in single crystals of MgVO and ZnVO. The usual settings of the EPR spectrometer are as follows: modulation field 1-5 G/100 kHz, microwave power 20 dB (max output power -200 mW). The EPR spectra were recorded in temperature range 120-300 K.

EPR spectra. Cu^{2+} EPR lines were observable at room temperature, however, they were strongly overlapped by the V^{4+} EPR lines, and it was not possible to identify them unambiguously. The large Cu^{2+} EPR linewidth is due to the overlapping Cu^{2+} lines, belonging to the ^{63}Cu and ^{65}Cu ions, and broadening due to the superhyperfine (SHF) interaction with the neighbouring ^{51}V nuclei ($I = 7/2$). Only one set of Cu^{2+} EPR lines was observed in ZnVO single crystal, as expected from its crystal structure, i.e. the Cu^{2+} ion occupies one physically inequivalent Zn^{2+} site, as seen from Fig. 2. To contrary, the Cu^{2+} ion occupies two physically inequivalent Mg^{2+} sites, Mg(1) and Mg(2), in MgVO, according to its structure, as seen from Fig. 3. However, only one set of angular variation of Cu^{2+} EPR line was observed. On other hand, some isotropic EPR lines were indeed observed in MgVO in temperature range from 120 K to 295 K, which can be assigned to the Cu^{2+} ion in second, probably Mg(2), crystallographical position. Detailed angular variations of the Cu^{2+} line positions were recorded at 120 K for variation of the magnetic field in 5° intervals in three mutually perpendicular planes (ZX, ZY, XY); Fig. 1, as these lines are clearly resolved at most orientations of magnetic field. They are shown in Fig. 4 and in Fig. 5 for MgVO and ZnVO, respectively. In both MgVO and ZnVO crystals, it was not possible to observe all four resolved hyperfine (HF) lines for several orientations of magnetic field, especially in ZX plane for MgVO. This is due to relatively small HF splitting, masked by the Cu^{2+} EPR linewidth.

Temperature variation of the EPR spectra. The EPR spectra for some chosen orientation of magnetic field in MgVO and ZnVO were recorded in the temperature range from 120 to 295 K as shown in Fig. 6a and Fig. 6b, respectively. As seen from these figures, there is no significant temperature dependence of the EPR linewidth of the Cu^{2+} ion in the temperature range 120 - 295 K. The average Cu^{2+} linewidth is about 30 G. The temperature dependence of integrated EPR lineshape of Cu^{2+} EPR lines follows the Curie law ($I_{\rm int} = C/T$) in temperature range 120 - 295 K. The isotropic EPR line with $g_1 = 2.38 \pm 0.01$ and $g_2 = 2.21 \pm 0.01$ were and, observed in the MgVO, are due to the Cu^{2+} ion at Mg(2) site undergoing Jahn-Teller effect.

Estimation of matrix elements of $\tilde{g}^2$- and $\tilde{A}^2$-tensors. The observed EPR line positions were simultaneously fitted to the spin-Hamiltonian appropriate to the site symmetry C_i, applicable to MgVO and ZnVO, expressed as follows [28]:

$$\mathbf{H} = \mu_{\rm B}\mathbf{B}\cdot\tilde{\mathbf{g}}\cdot\mathbf{S} + \mathbf{S}\cdot\tilde{\mathbf{A}}\cdot\mathbf{I}. \tag{1}$$

In Eq. (1), $\mu_{\rm B}$ is Bohr magneton, $\mathbf{B}$ is external magnetic field, $S = 1/2$ are the electronic spin and $I = 3/2$ nuclear spin of the Cu^{2+} ion, $\tilde{\mathbf{g}}$ is Zeeman matrix and $\tilde{\mathbf{A}}$ is the hyperfine (HF) interaction matrix. There are two isotope of Cu, each with $I = 3/2$: ^{63}Cu (natural abundance 69.09 %) and ^{65}Cu (natural abundance 30.91 %) nuclei [28]. Thus, each Cu^{2+} line splits into four hyperfine

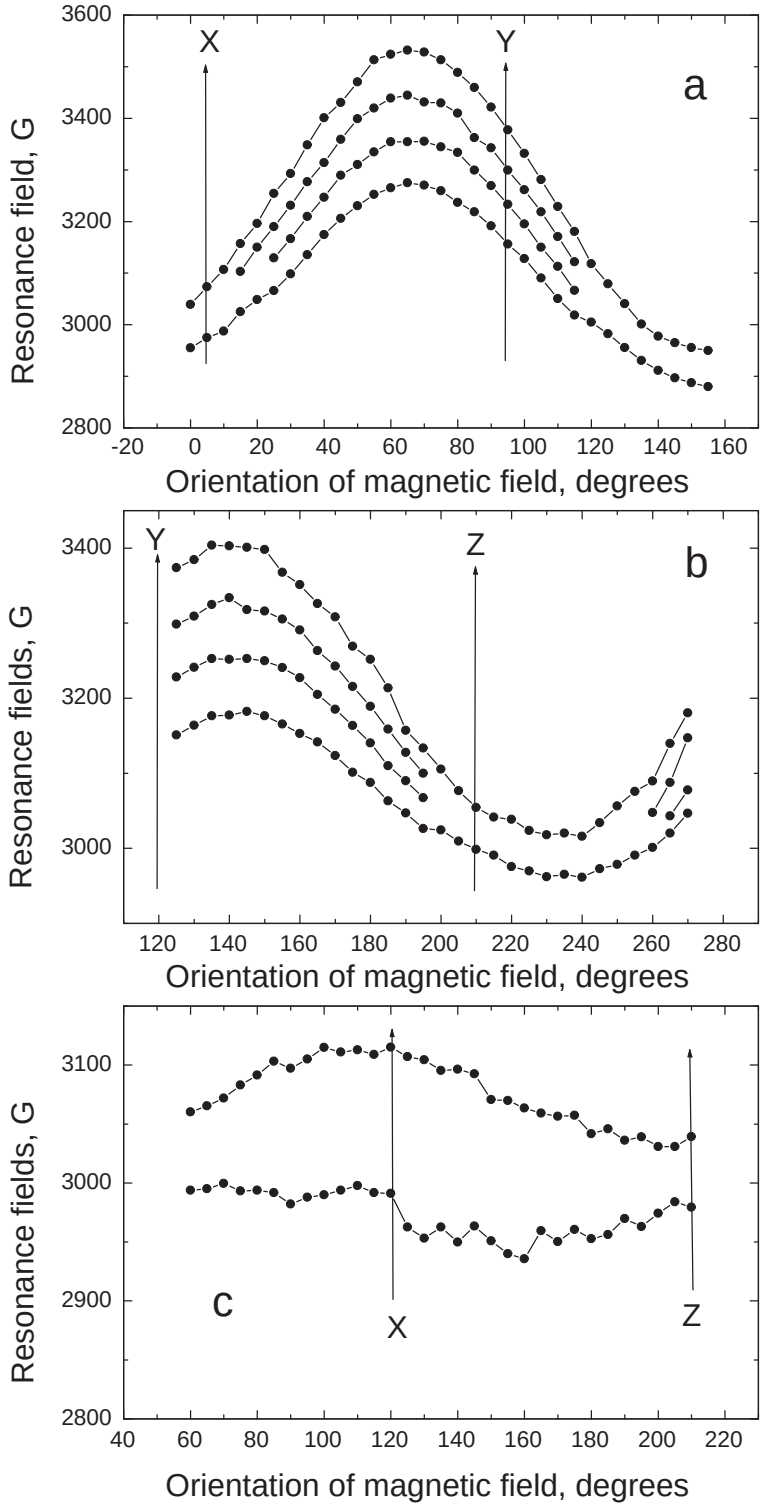

Figure 4. The angular variations of Cu^{2+} EPR resonance line positions in β-$Mg_2V_2O_7$ in three mutually perpendicular planes defined by the axes (X, Y, Z). Only outer HF lines were observed in XZ plane, other HF lines were not resolved.

(HF) lines at X-band, with the hyperfine lines of the two Cu isotopes overlapping each other within the linewidth. The quadrupolar-interaction terms are neglected in our consideration. In Eq. (1), the principal axes of the $\tilde{\mathbf{g}}$- and $\tilde{\mathbf{A}}$-matrices are here not coincident with each other, because of the low, monoclinic and triclinic, symmetries for ZnVO and MgVO, respectively, in

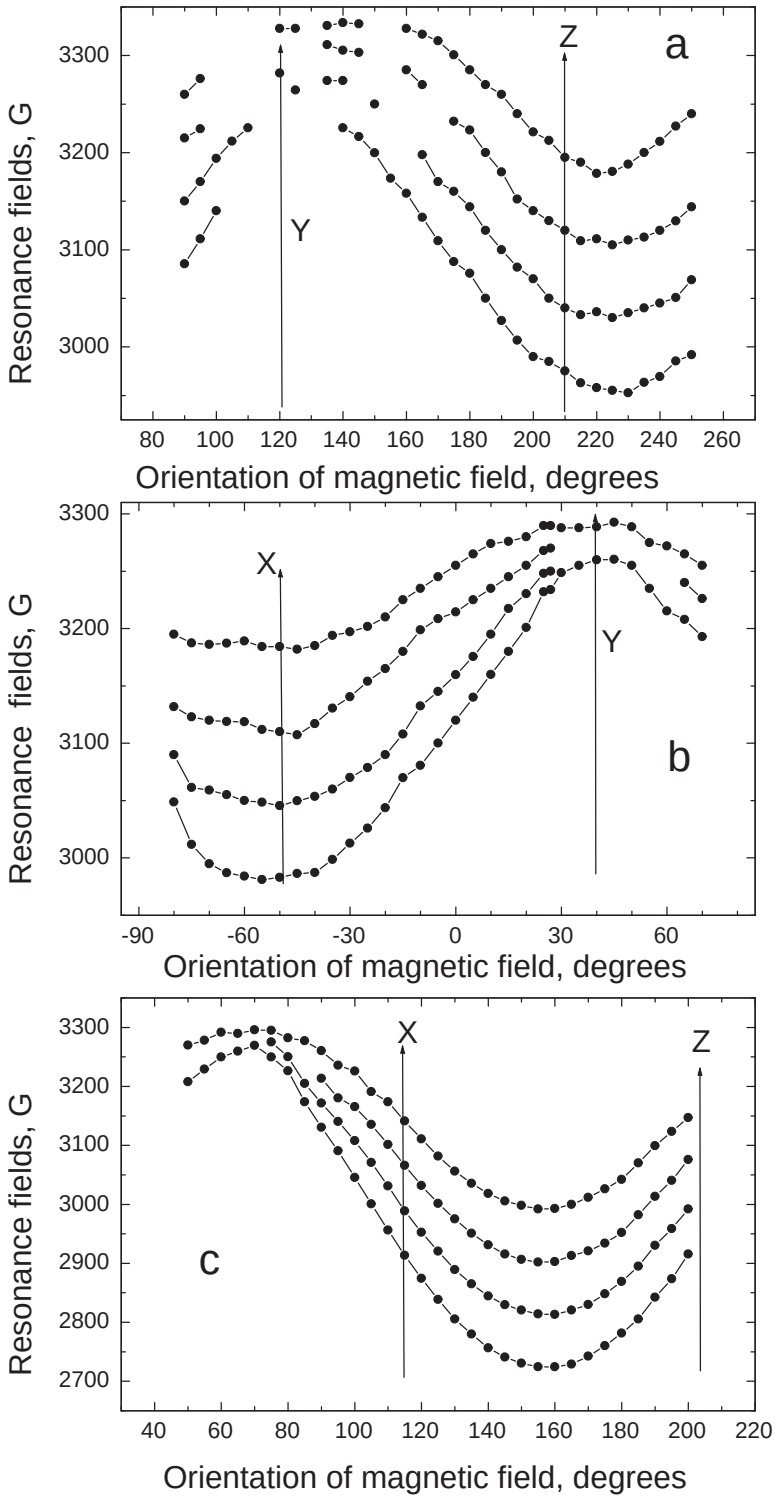

Figure 5. The angular variations of Cu^{2+} EPR resonance line positions in α-$Zn_2V_2O_7$ in three mutually perpendicular planes defined by the axes (X, Y, Z).

the present case, in agreement with the observed angular variations of EPR line positions. This complicates estimation of the $\tilde{\mathbf{g}}^2$- and $\tilde{\mathbf{A}}^2$-tensors accurately, unless a rigorous fitting procedure is used, as described below.

A rigorous least-squares fitting of all EPR line positions as observed in three mutually perpendicular planes was employed estimate $\tilde{\mathbf{g}}^2$- and $\tilde{\mathbf{A}}^2$-tensors, as described in [29–32]. It is first noted [32], that whereas $\tilde{\mathbf{g}}$ and $\tilde{\mathbf{A}}$ are matrices, $\tilde{\mathbf{g}}^2 = \tilde{\mathbf{g}}^{\mathrm{T}}\tilde{\mathbf{g}}$, $\tilde{\mathbf{A}}^2 = \tilde{\mathbf{A}}^{\mathrm{T}}\tilde{\mathbf{A}}$, are tensors, whose

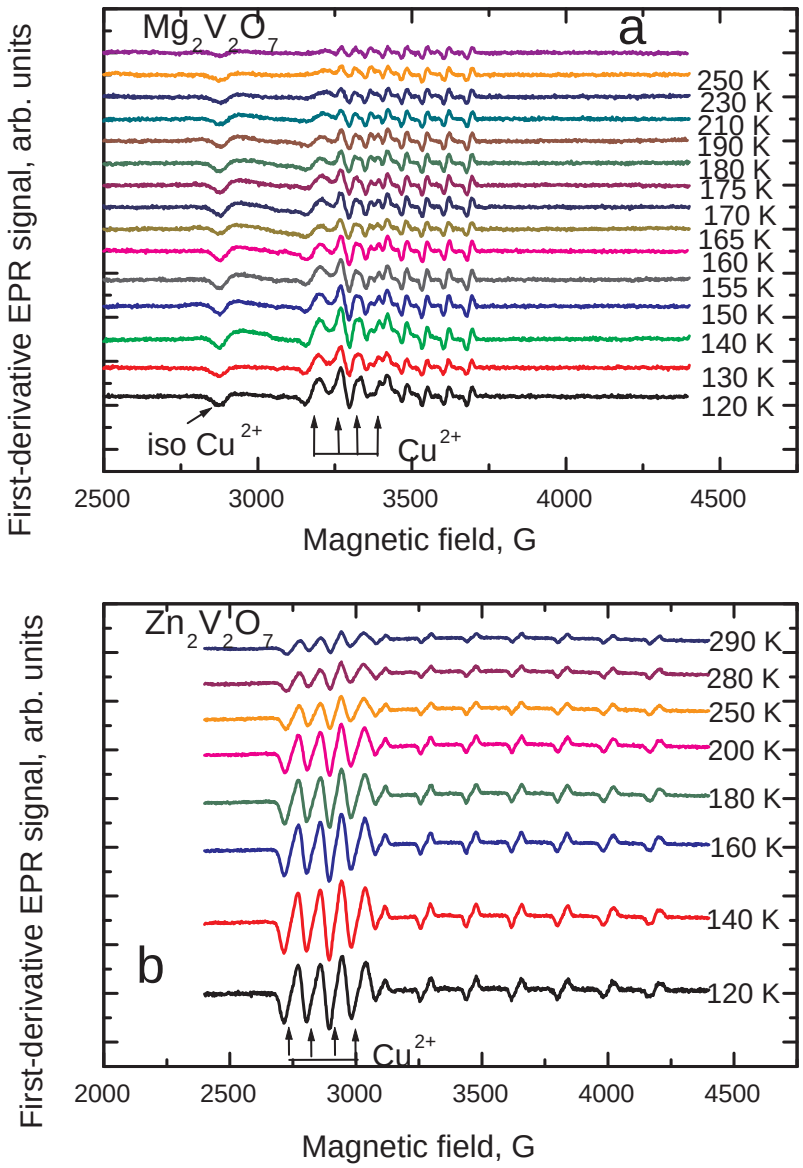

Figure 6. The temperature variations of Cu^{2+} EPR resonance line positions in β-$Mg_2V_2O_7$ at some chosen orientations in ZY and ZX planes, respectively. The "iso" in Fig. 6*a* refers to the isotropic Cu^{2+} line. The Cu^{2+} EPR lines are shown.

matrix elements are always symmetric, unlike those of the $\tilde{\mathbf{g}}$- and $\tilde{\mathbf{A}}$-matrices; which are not necessarily symmetric, here T denotes transpose of a matrix.

All the observed EPR line positions for the orientations of the magnetic field in the three mutually perpendicular planes ZX, ZY, XY, where the axes Z, X, Y are identified with respect to the crystal grown habits as shown in Fig. 1, were fitted simultaneously in a least-squares (LSF) manner as described in detail in [32]. In general, there were observed four hyperfine (HF) lines at each orientation of the magnetic field corresponding to the electronic spin $S = 1/2$ and the nuclear spin $I = 3/2$. The fitting was done in two successive procedures. First, the centres of each set of four HF lines were fitted to the six elements of the symmetric tensor $\tilde{\mathbf{g}}^2$. The 3×3 matrix for the $\tilde{\mathbf{g}}^2$-tensor was then diagonalized to obtain its principal values and directions cosines of the principal axes with respect to Z, X, Y-axes were determined. In the subsequent LSF procedure, all HF line positions as observed in the three mutually perpendicular planes were simultaneously fitted to the 12 parameters: the three principal values of $\tilde{\mathbf{g}}^2$-tensor, the

three Euler angles $(\vartheta, \varphi, \psi)$ and the six elements of the symmetric tensor $\tilde{\mathbf{A}}^2 = \tilde{\mathbf{A}}^{\mathrm{T}}\tilde{\mathbf{A}}$, using the eigenvalue expressions calculated to second-order in perturbation [30]. As for the initial values, the values already calculated for the principal values of the $\tilde{\mathbf{g}}^2$-tensor, and the Euler angles $(\vartheta, \varphi, \psi)$ as determined in the first procedure. As for the initial values for the six elements of the $\tilde{\mathbf{A}}^2$-tensor, they were chosen by trial-and-error until good fits were obtained as indicated by a minimum chi-squared value (SMD), defined in next paragraph. The minimum value of the SMD is calculated by successive iterations by varying the 12 parameters in the LSF manner. The 12 parameters, corresponding to the minimum of SMD, so obtained, enable one to calculate the principal values of the $\tilde{\mathbf{g}}$-matrix (square roots of principal values of the $\tilde{\mathbf{g}}^2$- tensor), the direction cosines of the $\tilde{\mathbf{g}}$-matrix with respect to the laboratory axes (the same as those of the $\tilde{\mathbf{g}}^2$-tensor), the three principal values of the $\tilde{\mathbf{A}}$-matrix, which are the square roots of the principal values of the $\tilde{\mathbf{A}}^2$-tensor as found by diagonalizing the matrix for the $\tilde{\mathbf{A}}^2$-tensor, which also yields the direction cosines of the $\tilde{\mathbf{A}}^2$-tensor, which are the same as those of the $\tilde{\mathbf{g}}$-matrix, with respect to the principal-axes of the $\tilde{\mathbf{g}}$-matrix. The listed values of the $\tilde{\mathbf{A}}^2$-tensor should be considered as averages of those estimated for the isotopes ^{63}Cu and ^{65}Cu, since the corresponding HF lines are not resolved from each other, due to larger linewidth.

The results of fitting for the principal values of $\tilde{\mathbf{g}}$-matrices for the MgVO and ZnVO are listed in the Table 1 and Table 2. In these Tables SMD $= \sum_i (\Delta E_i/h - \nu_i)^2$ is Square Mean Deviation, where $\Delta E_i/h$ is the calculated energy difference in GHz between the levels participating in resonance for the i-th line position, ν_i is the corresponding klystron frequency, h is Planck's constant. SMD is expressed in $(\mathrm{GHz})^2$. RSML $= (\mathrm{SMD}/n)^{1/2}$ is Root Mean Square deviation per Line and it is the average mean-square deviation of the calculated energy level difference in GHz from the energy of the microwave photon. The principal values of $\tilde{\mathbf{g}}$-matrix are dimensionless. The indicated errors are those estimated by the use of a statistical method as proposed [31]. The number of calculated EPR lines fitted to experimental EPR line positions under consideration is n. The direction cosines of $\tilde{\mathbf{g}}^2$- and $\tilde{\mathbf{A}}^2$-tensors with respect to the laboratory axes and with respect to the principal axes of the $\tilde{\mathbf{g}}^2$-tensor, respectively, for the two crystals are listed in Table 3 and Table 4. The principal axes of the $\tilde{\mathbf{g}}^2$-tensor are denoted as $Z'X'Y'$, whereas those of the $\tilde{\mathbf{A}}^2$-tensor with respect to $Z'X'Y'$ axes, are denoted as $Z''X''Y''$. The direction cosines of the principal axes of the $\tilde{\mathbf{g}}^2$-tensor X', Y', Z' are given with respect to the X, Y, Z-axes defined in section 2, while those of the $\tilde{\mathbf{A}}^2$-tensor, X'', Y'', Z'', are expressed relative to the principal axes of $\tilde{\mathbf{g}}^2$-tensor X', Y', Z'. The orientations of the principal magnetic axes $Z'X'Y'$ (i.e., those of the $\tilde{\mathbf{g}}^2$-tensor) of the Cu^{2+} impurity ions are found to be coincident with those of the Mn^{2+} ions in ZnVO [20]. In particular, the principal magnetic axes Z' and X' lie in the plane perpendicular to the [110] cleavage plane of the crystal, and Y' axis is parallel to the [001] crystallographic axis. The orientation of principal magnetic axes $Z'X'Y'$, i.e. those of the $\tilde{\mathbf{g}}^2$-tensor of the Cu^{2+} impurity ions, relative to the laboratory coordinate system ZXY in MgVO are not coincident with these. It is noted from Table 1 and Table 2 that the principal values of the $\tilde{\mathbf{g}}^2$-tensors are almost the same for these two pyrovanadates, whereas the principal values of $\tilde{\mathbf{A}}^2$-tensors are very close to each other. However, the orientations of the principal axes of the $\tilde{\mathbf{g}}^2$-tensors for these crystals are oriented quite different relative to the laboratory axes XYZ. The same is a

Table 1. The principal values of $\tilde{\mathbf{g}}$-matrices of the Cu^{2+} ion in MgVO and ZnVO single crystals at 120 K.

	g_z	g_x	g_y	n	SMD	RSML
β-$Mg_2V_2O_7$	2.015±0.001	2.283±0.001	2.358±0.001	93	0.16	0.04
α-$Zn_2V_2O_7$	1.999±0.001	2.283±0.001	2.358±0.001	96	0.09	0.03

Table 2. The principal values of $\tilde{\mathbf{A}}$-matrices, expressed in GHz, of the Cu^{2+} ion in MgVO and ZnVO single crystals at 120 K.

	A_z, GHz	A_x, GHz	A_y, GHz	n	SMD	RSML
β-$Mg_2V_2O_7$	0.24±0.01	0.13±0.01	0.00±0.01	210	39	0.41
α-$Zn_2V_2O_7$	0.26±0.01	0.17±0.01	0.00±0.01	235	16	0.26

Table 3. The direction cosines of $\tilde{\mathbf{g}}^2$- and $\tilde{\mathbf{A}}^2$-tensors of the Cu^{2+} ion in MgVO at 120 K. The principal axes of the $\tilde{\mathbf{g}}^2$-tensor are denoted as $Z'X'Y'$, whereas those of the $\tilde{\mathbf{A}}^2$-tensor with respect to $Z'X'Y'$ axes are denoted as $Z''X''Y''$.

$\tilde{\mathbf{g}}^2$-tensor				$\tilde{\mathbf{A}}^2$-tensor			
	Z'	Y'	X'		Z''	Y''	X''
Z	−0.2137	0.9481	−0.2355	Z'	0.5309	−0.7042	−0.4713
Y	0.5291	0.3150	0.787	Y'	0.6624	0.6918	−0.2874
X	0.8212	0.4376	−0.5689	X'	0.5285	−0.1596	0.8338

Table 4. The direction cosines of $\tilde{\mathbf{g}}^2$- and $\tilde{\mathbf{A}}^2$-tensors of the Cu^{2+} ion in ZnVO at 120 K. The principal axes of the $\tilde{\mathbf{g}}^2$-tensor are denoted as $Z'X'Y'$, whereas those of the $\tilde{\mathbf{A}}^2$-tensor with respect to $Z'X'Y'$ axes are denoted as $Z''X''Y''$.

$\tilde{\mathbf{g}}^2$-tensor				$\tilde{\mathbf{A}}^2$-tensor			
	Z'	Y'	X'		Z''	Y''	X''
Z	0.2030	0.6585	0.7247	Z'	0.8865	−0.2269	0.4033
Y	−0.4907	−0.5720	0.6572	Y'	0.4425	0.1610	−0.8822
X	0.8473	−0.4890	0.2070	X'	0.1353	0.9605	0.2432

true for the orientations of the principal axes of the $\tilde{\mathbf{A}}^2$-tensors. This result is in deviance from that for the V^{4+} ions in these two pyrovanadate [21], where the principal values of the $\tilde{\mathbf{g}}^2$- and $\tilde{\mathbf{A}}^2$-tensors, as well as the orientation of the principal axes of $\tilde{\mathbf{g}}^2$- and $\tilde{\mathbf{A}}^2$-tensors are similar to each other in these two crystals.

The ground state of the Cu^{2+}. For the ground state $|0\rangle$, $g_{\|} = 2.0$, $g_{\perp} = 2 - 6\lambda/\Delta_2$ [28], where λ is spin orbital coupling constant, and Δ_2 is the splitting of d^9 configuration of the Cu^{2+} ion between $|0\rangle$ and $|\pm 1\rangle$ levels in an octahedral field, with tetragonal or trigonal distortion. Now, the typical value of $\lambda/\Delta \approx -0.05$, where Δ is splitting between e_g and t_{2g} levels in octahedral field; $\Delta \approx \Delta_2 \approx 10\,Dq$, therefore, one has $g_{\|} = 2.0$ and $g_{\perp} \approx 2.3$; $g_{\perp} = (g_x + g_y)/2$ [28]. Similar values were obtained from the experimental data for the Cu^{2+} ion in both MgVO and ZnVO crystals. Zaripov and Chirkin [33] analyzed electronic structure of different transition metal ions, including Cu^{2+} in low symmetry environment. However, such analysis requires the knowledge of the signs of A- parameters, which is not possible with the present EPR data, because of lack of liquid-helium temperature measurements.

4. Conclusions

The salient features of the Cu^{2+} EPR investigations of MgVO and ZnVO single crystals as follows:

1. The principal values of the $\tilde{\mathbf{g}}^2$- and $\tilde{\mathbf{A}}^2$-tensors of the Cu^{2+} ions and the orientations of the principal axes of the $\tilde{\mathbf{g}}^2$-tensors, have been determined in MgVO and ZnVO crystals at 120 K using a rigorous least-squares fitting (LSF) procedure.

2. The principal values of the $\tilde{\mathbf{g}}^2$- and $\tilde{\mathbf{A}}^2$-tensors of the Cu^{2+} ion in MgVO and ZnVO single crystals are found to have similar values, implying that the Cu^{2+} ions have the same ground state, $|0\rangle$, in the two crystals.

3. The Mg^{2+} and Zn^{2+} ions are differently coordinated in these host crystals. The Cu^{2+} ion is 6-fold coordinated in MgVO, whereas it is 5-fold coordinated in ZnVO in trigonalal bipyramidal coordination. As a consequence, the Cu^{2+} ions that substitute for these cations have non-coincident orientations of the principal axes of their $\tilde{\mathbf{g}}^2$- and $\tilde{\mathbf{A}}^2$-tensors in these two crystals. The LSF procedure used here is capable of determining the non-coincident orientations of the principal axes of the $\tilde{\mathbf{g}}^2$- and $\tilde{\mathbf{A}}^2$-tensors in the two crystals.

Acknowledgments

This research was supported by the Natural Sciences and Engineering Research Council of Canada (NSERC)(SKM). SIA is grateful for a partial financial support in the frame of research project, allocated to Kazan Federal University, Russia, from the Russian Ministry of Education and Science (3.2166.2017/4.6).

References

1. Blasco T., Nieto J. M. L. *Appl. Catal.* **A157**, 117 (1997).

2. Busca G., Lietti L., Ramis G., Betti F. *Appl. Catal.* **B18**, 1 (1998).

3. Zhang S., Zhong Q. *J. Solid. State. Chem.* **221**, 49 –56 (2015).

4. Blasco T., Nieto J. M. L., Dejoz A., Vazquez M. *J. Catal.* **157**, 271 (1995).

5. Thompson K., McNeill J., Orvig C. *Chem. Rev.* **99**, 2561 (1999).

6. Pistoia G., Wang G., D. D. Z. *Solid State Ionic* **76**, 285 (1995).

7. Kong F. Y., Li M., Yao X., Xu J., Wang A., Liu Z., Li G. *Cryst. Eng. Commun.* **14**, 3858 (2012).

8. Pan A., Wu H. B., Yu L., Lou X. W. *Angew. Chem. Int. Ed.* **52**, 2226 (2013).

9. Zhu J., Cao L., Wu Y., Gong Y., Liu Z., Hoster H., Zhang Y., Zhang S., Yang S., Yan Q., Ajayan P., Vajtai R. *Nano Lett.* **13**, 5408 (2013).

10. Mori K. *J. Soc. Powder Technol. Japan* **41**, 750 (2004).

11. Yu M., Liu X., Wang Y., Zheng Y., Zhang J., Li M., Lan W., Su Q. *Appl. Surf. Sci.* **258**, 9554 (2012).

12. Brown J., Hummel F. *Trans. Brit. Ceram. Soc.* **64**, 419 (1965).

13. Ioffe V., Grunin V., Zonn Z., Ivanov S., Yanchevskaya I. *Izv. Akad Nauk SSSR, Neorg. Mater.* **13**, 1484 (1977).

14. Ioffe V., Moskalev V., Dmitrieva L., Ivanov S., Zonn Z. *Sov. Phys. Solid. State.* **17**, 2043 (1976).

15. Andronenko S., Dmitrieva L., Molodchenko N., Moskalev V., Zonn Z. *Inorg. Chem.* **21**, 535 (1979).

16. Nielsen V., Jakobsen H., Skibsted J. *J. Phys. Chem. B* **105**, 420 (2001).

17. Lo A., Hanna J., Schurko R. W. *Appl. Magn. Res.* **32**, 691 (2007).

18. Stager C. *Can. J. Phys.* **46**, 807 (1968).

19. Ioffe V., Andronenko S., Zonn Z. in *Magnetic resonance and related phenomena: Proc. of the XX th congress AMPERE*, edited by Kundla E., Lippmaa E., Saluvere T. (Springer-Verlag Berlin Heidelberg, Tallinn, 1979) p. 305.

20. Misra S., Andronenko S., Earle K., Freed J. *Appl. Magn. Reson.* **21**, 549 (2001).

21. Misra S., Andronenko S. *Magn. Reson. Solids* **20**, 18101(8p) (2018).

22. Guimond S., Haija M. A., Kaya S., Lu J., Weissenrieder J., Shaikhutdinov S., Kuhlenbeck H., Freund H.-J., Döbler J., Sauer J. *Top. Catal.* **38**, 117 (2006).

23. Xia Q., Obana Y., Nishiguchi H., Ito M., Ishihara T., Takita Y. *J. Jpn. Petrol. Inst.* **46**, 87 (2003).

24. Shannon R. *Acta Crystallogr. A* **32**, 751 (1976).

25. Gopal R., Calvo C. *Can. J. Chem.* **51**, 1004 (1973).

26. Krasnenko T., Vasyutinskaya E., Zolotukhina L., Dobrynin B., Slobodin B. *Russian Journal of Inorganic Chemistry* **46**, 733 (2001).

27. Gopal R., Calvo C. *Acta Cryst.B* **30**, 2491 (1974).

28. Abragam A., Bleaney B. *Electron Paramagnetic Resonance of Transition Ions* (Clarendon Press, Oxford, 1970).

29. Misra S. *J. Magn. Reson.* **23**, 403 (1976).

30. Misra S. *Physica B* **151**, 433 (1988).

31. Misra S., Subramanian S. *J. Phys. C.: Sol. St. Phys.* **15**, 7199 (1982).

32. Misra S. *Physica B+C* **124**, 53 (1984).

33. Zaripov M., Chirkin G. in *Paramagnetic Resonance*, 3, edited by Altshuler S. (Kazan State University, Kazan, 1968) pp. 55–99, [in Russian].